

Neck retardation and enhanced energy absorption in metal–elastomer bilayers

Zhenyu Xue *, John W. Hutchinson

Division of Engineering and Applied Sciences, Harvard University, 29 Oxford St, Pierce 316, Cambridge, MA 02138, United States

Received 29 September 2005

Abstract

Retardation of necking under biaxial stretching of bilayer plates comprised of an elastomer layer bonded to a metal layer is studied. Substantial increases in necking limits and consequent energy absorption can be achieved in metal–elastomer bilayers for both quasi-static and dynamic stretching. The phenomena is tied to the fact that under stretching the incremental modulus of the elastomer remains essentially unchanged, or increases, while the incremental modulus of the metal steadily decreases. The effective incremental modulus of the bilayer decreases with stretching but at a lower rate than the metal itself. Since necking instabilities are associated with an erosion of the incremental modulus, necking in the bilayer is delayed to larger strains. Although the strength of a bilayer having the same mass/area as an all-metal plate is reduced, it can nevertheless absorb more energy than the metal plate if the ratio of the elastomer modulus to metal yield stress is sufficiently large. The first part of the paper derives necking limits and energy absorption capacities for bilayers under quasi-static biaxial stretching. The second part of the paper analyses axisymmetric neck development in clamped circular bilayers subject to impulsive pressure loads. The ability of the bilayer to sustain intense impulses is compared to the performance of metal plates of the same material and total mass. Outstanding issues requiring further study are discussed.

© 2006 Elsevier Ltd. All rights reserved.

Keywords: Bilayers; Elastomer–metal plates; Necking; Rupture; Forming limit diagram; Impulsive loads

1. Introduction

Rupture of ductile metal plates or sheets subject to in-plane biaxial stretching often begins with the onset of necking. As necking proceeds, deformation outside the neck ceases while localized deformation

within the neck gives rise to large local strains coupled with increased stress triaxiality, both of which promote ductile fracture. In uniaxial tension, the onset of necking in a uniform tensile member occurs when the true stress equals the tangent modulus of the true stress–strain curve—the Considere Criterion. For a metal described by power hardening with strain hardening exponent, N , the true strain at the onset of necking in a bar in uniaxial tension is $\varepsilon = N$. This is also the necking strain for a metal

* Corresponding author. Tel.: +1 617 4965167; fax: +1 617 4960601.

E-mail address: xue@esag.harvard.edu (Z. Xue).

plate or thin sheet that is subject to plane strain tension wherein one of the in-plane strain components is constrained to be zero.

Of interest in this paper is the role in retarding the onset of necking of an elastomer layer bonded to the metal sheet or plate. Neck retardation allows the bilayer to be stretched to larger overall strains, potentially permitting greater energy absorption. In the range of strains of relevant to metal necking, the incremental modulus of many elastomers remains constant or even increases slightly with stretching while the incremental modulus of the metal decreases steadily. Compared to a single metal plate at a given level of stretch, the bilayer has lower average stress and higher tangent modulus, both of which promote neck retardation. This is the essence of the phenomenon. It will be seen that bilayer combinations exist which absorb considerably more energy under stretching than the corresponding single metal sheet having the same mass/area. The effect occurs under both quasi-static and dynamic stretching, although inertia and material strain-rate dependence become important in the latter case. This is a significant phenomenon for plate structures designed to survive high intensity impulsive loads without rupture. The second part of the paper investigates whether metal–elastomer bilayers exist which are more effective at withstanding a given impulsive load than all-metal plates of comparable mass.

The first part of the paper revisits the basic mechanics of necking bifurcation by considering the onset of necking in bilayers subject to arbitrary combinations of quasi-static in-plane stretching. Necking limit diagrams, analogous to forming limit diagrams used in the sheet metal industry, are obtained as a function of the material properties and the relative thicknesses of the layers. Curves showing the effectiveness of the elastomer in enhancing energy absorption are also presented.

The second part of the paper focuses on a specific problem where energy absorption is critical—high intensity impulsive loading of clamped circular plates. The role of the elastomer layer in promoting neck retardation under dynamic stretching is also demonstrated, although the phenomenon becomes more complicated due to the contributing role of inertia in retarding necking in the absence of the elastomer layer. Results are presented which show that bilayers can withstand higher impulses than an all-metal plate having the same mass. Issues requiring further attention are also discussed.

2. The onset of necking in bilayer plates subject to quasi-static biaxial stretching

The strains at which necking occurs are sufficiently large such that elasticity and compressibility of the metal can be neglected. A power law will be used to represent the relation between the true stress and logarithmic strain of the metal in uniaxial tension according to

$$\sigma = \sigma_R \varepsilon^N \quad (1)$$

where σ_R is the flow stress extrapolated to a strain of unity and N is the strain hardening exponent. A finite strain deformation theory of plasticity will be used to generalize (1) to multi-axial stress states (Hutchinson and Neale, 1978). Let λ_i ($i = 1, 3$) be the principal stretches with $\varepsilon_i = \ln \lambda_i$ as the principal logarithmic strains. With $\varepsilon_{\text{eff}} = (2\varepsilon_i\varepsilon_j/3)^{1/2}$ as the effective strain, the work density to deform the metal is

$$W_m = \frac{1}{N+1} \sigma_R \varepsilon_{\text{eff}}^{N+1} \quad (2)$$

The principal stresses are obtained from $\sigma_i = \partial W_m / \partial \varepsilon_i - p$, where p is the hydrostatic pressure and the incompressibility constraint is $\varepsilon_1 + \varepsilon_2 + \varepsilon_3 = 0$.

The Mooney–Rivlin relation for incompressible rubber-like materials will be used to describe the elastomer. The strain energy density in terms of the principal stretches is

$$W_e = c_1(\lambda_1^2 + \lambda_2^2 + \lambda_3^2 - 3) + c_2(\lambda_1^2\lambda_2^2 + \lambda_1^2\lambda_3^2 + \lambda_2^2\lambda_3^2 - 3) \quad (3)$$

with the constraint $\lambda_1\lambda_2\lambda_3 = 1$ and with principal stresses given by $\sigma_i = \lambda_i \partial W_e / \partial \lambda_i - p$ (no summation). Experimental data for polyurea, an elastomer that will be considered in Section 3, indicates that $|c_2| \ll |c_1|$ (Amirkhizi et al., 2006; McGee et al., 2005; and Appendix of the present paper). To limit the number of parameters considered in this section, we take $c_2 = 0$. Then, $c_1 = E/6$, where E is Young's modulus (at zero strain), and the tensile stress–strain relation is neo-Hookean:

$$\sigma = \frac{E}{3} (e^{2\varepsilon} - e^{-\varepsilon}) \quad (4)$$

Necking under arbitrary combinations of principal in-plane tensile strains, ε_1 and ε_2 , is considered, and without loss of generality one can take $\varepsilon_1 \geq \varepsilon_2 \geq 0$. Under these conditions, the necking band lies perpendicular to the x_1 -direction, and the only two non-zero stress components in a long

wavelength, plane stress bifurcation analysis of necking in a sheet or thin plate are σ_1 and σ_2 . Define incremental moduli relating increments of the non-zero true stresses to increments of the logarithmic strains, ε_1 and ε_2 , such that

$$\dot{\sigma}_\alpha = L_{\alpha\beta} \dot{\varepsilon}_\beta \quad (\alpha = 1, 2; \beta = 1, 2) \quad (5)$$

with summation on a repeated index. In the analysis of the onset of necking in bands perpendicular to the x_1 -direction, only L_{11} is needed. For the metal (Hutchinson and Neale, 1978),

$$L_{11}^m = \frac{4}{3} E_s - (E_s - E_t) \left(\frac{\sigma_1^2}{\sigma_{\text{eff}}^2} \right) \quad (6)$$

where $\sigma_{\text{eff}} = \sqrt{\sigma_1^2 - \sigma_1 \sigma_2 + \sigma_2^2}$, $E_s = \sigma_R \varepsilon_{\text{eff}}^{N-1}$ and $E_t = N \sigma_R \varepsilon_{\text{eff}}^{N-1}$. For the elastomer,

$$L_{11}^e = \frac{2}{3} E (e^{2\varepsilon_1} + e^{-2(\varepsilon_1 + \varepsilon_2)}) \quad (7)$$

Consider uniform proportional stretching of the bilayer prior to necking with $\varepsilon_2 = \psi \varepsilon_1$ where ψ is held constant and is in the range $0 \leq \psi \leq 1$. Denote the current thicknesses of the metal and elastomer plates by h^m and h^e , respectively, with initial values, h_0^m and h_0^e . Define the relative thickness of each layer as a fraction of the total bilayer thickness by $f^m = h^m / (h^m + h^e)$ and $f^e = h^e / (h^m + h^e)$. These do not change as the bilayer undergoes plane stress deformation because ε_3 is the same in each layer due to the fact that the layers experience the same in-plane strains and the materials are incompressible. Thus, in terms of the initial thickness ratio, h_0^e / h_0^m ,

$$f^m = 1 / (1 + h_0^e / h_0^m), \quad f^e = 1 - f^m \quad (8)$$

The stresses and incremental moduli averaged through the bilayer satisfy

$$\begin{aligned} \dot{\bar{\sigma}}_\alpha &= \bar{L}_{\alpha\beta} \dot{\bar{\varepsilon}}_\beta \quad \text{where } \bar{\sigma}_\alpha = f^m \sigma_\alpha^m + f^e \sigma_\alpha^e \\ \text{and } \bar{L}_{\alpha\beta} &= f^m L_{\alpha\beta}^m + f^e L_{\alpha\beta}^e \end{aligned} \quad (9)$$

Let $F = \bar{\sigma}_1 (h^m + h^e)$ be the force/length acting in the x_1 -direction across sections through the bilayer parallel to the x_2 -direction. The bifurcation condition for the onset of a necking band parallel to the x_2 -direction is $\dot{F} = 0$ for bifurcation strain increments constrained to satisfy $\dot{\varepsilon}_2 = 0$ in the band (Storen and Rice, 1975; Hutchinson and Neale, 1978). In the present case, the bifurcation condition is simply $\bar{\sigma}_1 = \bar{L}_{11}$, which by (6)–(9), is satisfied when

$$\begin{aligned} S &(e^{2\varepsilon_1} + 3e^{-2(1+\psi)\varepsilon_1}) \\ &= \varepsilon_{\text{eff}}^{N-1} \left[2(2 + \psi)\varepsilon_1 + \frac{(1 - N)(2 + \psi)^2}{(1 + \psi + \psi^2)} - 4 \right] \end{aligned} \quad (10)$$

where $\varepsilon_{\text{eff}} = 2(1 + \psi + \psi^2)^{1/2} \varepsilon_1 / \sqrt{3}$ and

$$S = \frac{h_0^e E}{h_0^m \sigma_R} \quad (11)$$

Results for a single metal layer will be reviewed before addressing the role of the elastomer in the bilayer. With $S = 0$, condition (10) reduces to

$$\varepsilon_1 = \frac{3\psi^2 + N(2 + \psi)^2}{2(2 + \psi)(1 + \psi + \psi^2)} \quad (12)$$

This is the strain at the onset of necking under biaxial tensile stretching obtained by Storen and Rice (1975). The result is sensitive to the specific multi-axial constitutive law used to characterize the metal due to the abrupt change in direction of plastic flow at bifurcation. Under overall biaxial tensile straining, $\dot{\varepsilon}_2 = \psi \dot{\varepsilon}_1$ prior to necking, while the bifurcation strain increments in the band must satisfy $\dot{\varepsilon}_2 = 0$. For $\psi > 0$, necking strains at bifurcation predicted using a conventional theory based on the Mises yield surface are found to be excessively large due to the constraint on the direction of plastic flow imposed by the yield surface. As noted in the derivation above, (10) and (12) are based on a deformation theory of plasticity, which permits an abrupt change in the direction of plastic flow in the necking band when bifurcation occurs. Under in-plane plane strain stretching ($\psi = 0$), (12) reduces to $\varepsilon_1 = N$; this special case does not involve an abrupt change in flow direction, and it is insensitive to choice of constitutive model. Further background on this issue is given by Storen and Rice and by Hutchinson and Neale (1978), including discussion of evidence that necking predictions based on the deformation theory give realistic agreement with experiments.

A plot of combinations of the in-plane logarithmic strains corresponding to the onset of necking is referred to as a “forming limit diagram” in the sheet metal forming industry. This diagram plays a central role in designing stretching processes for forming of metal sheets and thin plates. An example of a forming limit diagram for a single-layer metal sheet with strain hardening exponent, $N = 0.2$, is given in Fig. 1 as the curve labeled $S = 0$. As noted above, the neck is perpendicular to the maximum

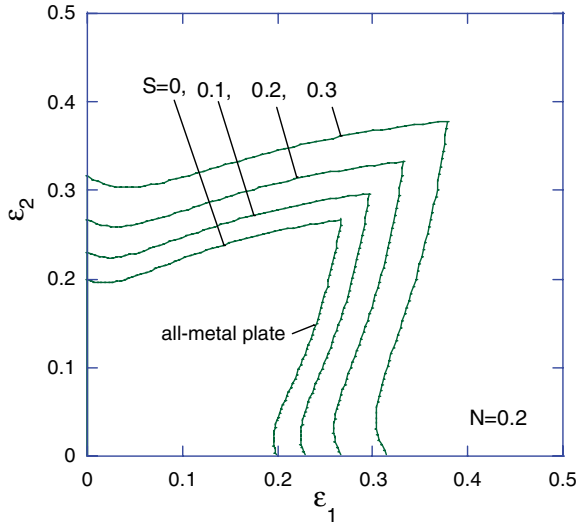


Fig. 1. Strains at the onset of necking in bilayer plates subject to biaxial tensile stretching. The metal layer has strain hardening exponent $N = 0.2$, reference strength σ_R and initial thickness h_0^m . The elastomer layer has modulus E and initial thickness h_0^e . The stiffness-strength parameter is $S = h_0^e E / h_0^m \sigma_R$.

principal strain. For $\varepsilon_2 \geq \varepsilon_1$, the roles of the two strain components have been switched in the above formulas, providing the second branch of the strain contours in Fig. 1. The corner on the necking limit contours at the orientation transition ($\varepsilon_1 = \varepsilon_2$) corresponds to equi-biaxial stretching; for this strain state the neck can have any orientation.

The necking strain in the bilayer depends on only three parameters: the strain ratio, ψ ; the strain hardening exponent, N ; and the bilayer stiffness-strength ratio, S . Fig. 1 includes contours from (10) corresponding to the onset of necking for four values of S . The extent to which necking is retarded by the elastomer layer under plane strain stretching ($\psi = 0$) and equi-biaxial stretching ($\psi = 1$) is plotted in Fig. 2. Neck retardation becomes significant when $S \approx 0.1$, and the necking strain is more than doubled when $S = 0.5$. Because S depends on the ratio of the thicknesses of the layers making up the bilayer, in principle, the necking strain can be increased by an arbitrarily large factor by trading metal for elastomer keeping the total mass of the bilayer fixed. The question then becomes how the strength and energy absorption of the bilayer change as elastomer is substituted for metal.

One way to make a meaningful assessment of the performance of bilayer is to compare it with a single-layer plate made of the same metal and having the same mass/area as the bilayer. Let ρ^m and ρ^e

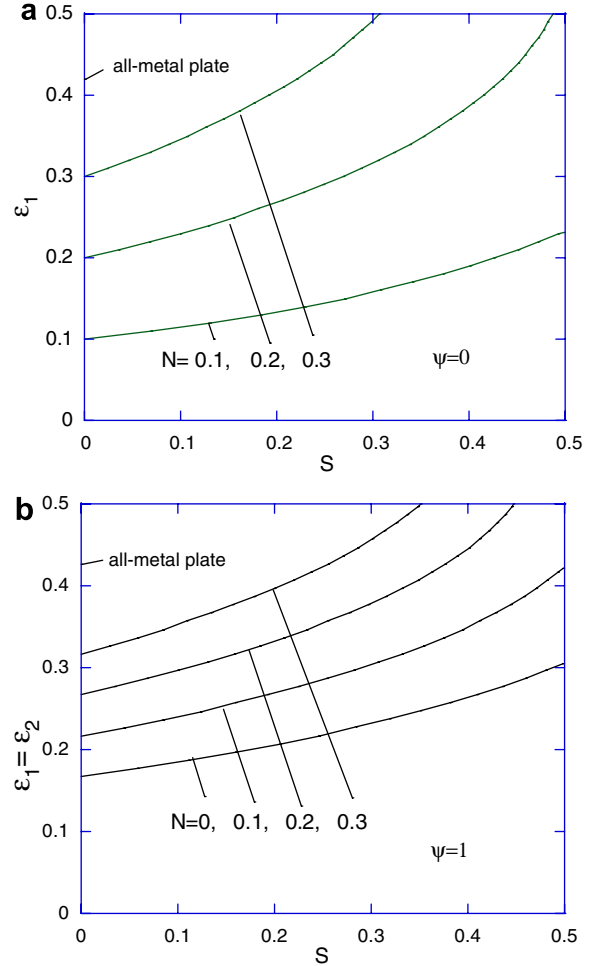


Fig. 2. Strain at the onset of necking for bilayer plates as a function of the stiffness-strength parameter, $S = h_0^e E / h_0^m \sigma_R$: (a) plane strain tension, $\psi = 0$; (b) equi-biaxial tension, $\psi = 1$.

be the densities of the metal and elastomer, respectively, and let H_0^m be the initial thickness of the all-metal plate. Plates with the same mass per initial area, m_0 , have

$$m_0 = \rho^m h_0^m + \rho^e h_0^e = \rho^m H_0^m \quad (13)$$

The energies per initial area absorbed by the all-metal plate and the bilayer prior to necking are

$$\begin{aligned} U_{\text{metal plate}} &= H_0^m W_m, \\ U_{\text{bilayer plate}} &= h_0^m W_m + h_0^e W_e \end{aligned} \quad (14)$$

evaluated at their respective necking strains. For the two plates having the same mass/area, the ratio of the absorbed energies is

$$\frac{U_{\text{bilayer plate}}}{U_{\text{metal plate}}} = \left(1 + \frac{h_0^e}{h_0^m}\right) \left(1 + \frac{\rho^e}{\rho^m} \frac{h_0^e}{h_0^m}\right)^{-1} \times \frac{(f^m W_m + f^e W_e)_{\text{bilayer plate}}}{(W_m)_{\text{metal plate}}} \quad (15)$$

evaluated at the respective necking strains. This ratio is a function of the five dimensionless parameters: h_0^e/h_0^m , ψ , N , ρ^e/ρ^m and E/σ_R . A plot of this ratio is presented in Fig. 3a for plate strain stretching ($\psi = 0$) for a representative combination of elastomer ($\rho^e = 1100 \text{ kg m}^{-3}$) and steel ($\rho^m = 7800$

kg m^{-3} , $N = 0.2$). The ratio of the elastomer modulus to steel strength, E/σ_R , is treated as a variable. By substituting elastomer for steel with no increase in overall mass, the bilayer plate is able to absorb more energy prior to the onset of necking than the metal plate if $E/\sigma_R > 0.1$. The comparison under equi-biaxial stretching ($\psi = 1$) is similar, as seen in Fig. 3b. The role of both the strain hardening exponent of the metal, N , and modulus-strength ratio, E/σ_R , on the energy absorption ratio (15) is displayed in Fig. 4 for bilayers having equal metal and elastomer thicknesses. Metal layers having high

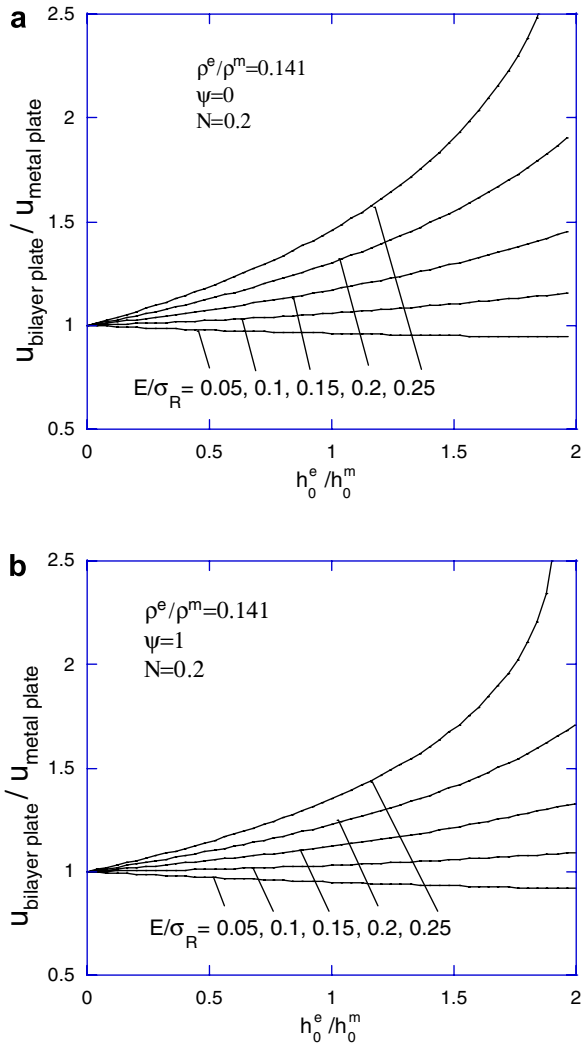


Fig. 3. Ratio of the energy dissipated at the onset of necking for a bilayer plate to that of an all-metal plate of the same mass/area as a function of the initial thickness of the metal layer in the bilayer to the initial thickness of the all-metal plate. The density ratio is representative of an elastomer-steel bilayer: (a) plane strain tension, $\psi = 0$; (b) equi-biaxial tension, $\psi = 1$.

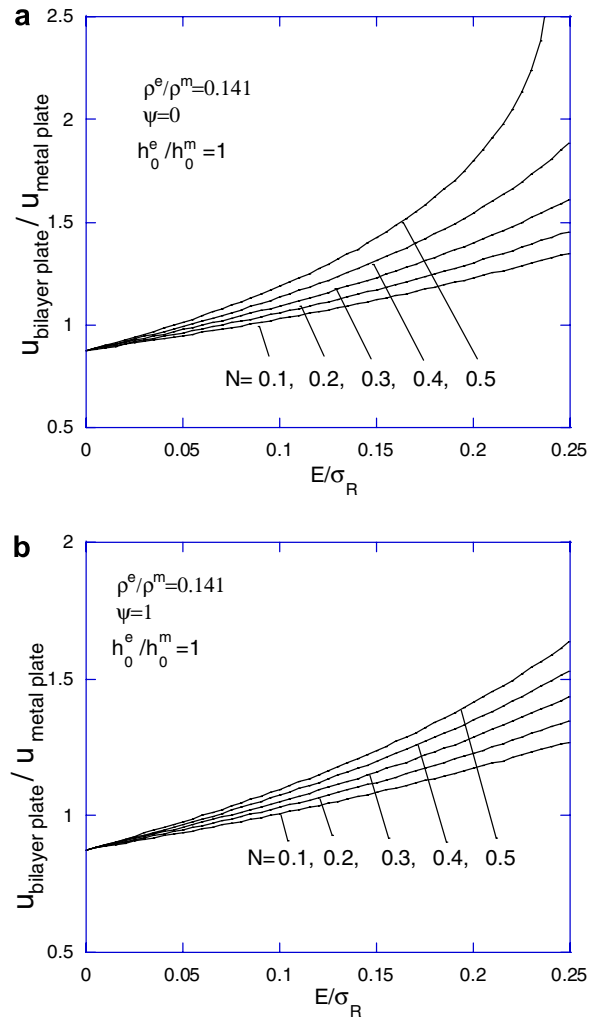


Fig. 4. Ratio of the energy dissipated at the onset of necking for a bilayer plate to that of an all-metal plate of the same mass/area as a function the ratio of elastomer modulus to metal reference stress for various metal strain hardening exponents. The thicknesses of the metal and elastomer layers in the bilayer are equal: (a) plane strain tension, $\psi = 0$; (b) equi-biaxial tension, $\psi = 1$.

strain hardening exponent show the largest amplification of energy absorption. Although energy absorption in the bilayer relative to the all-metal plate is slightly larger in plane strain tension than in equi-biaxial tension, the minimum value of the modulus-strength ratio required for a significant benefit ($E/\sigma_R \approx 0.1$) is essentially independent of the in-plane strain ratio ψ .

Under plane strain stretching ($\psi = 0$), $\dot{\varepsilon}_2 = 0$ holds inside and outside the band throughout the entire history. Thus, for $\psi = 0$, the onset of necking is associated with the maximum of the curve of force/length, F , as a function of ε_1 , in exact analogue to the Considere criterion for necking of a bar in tension. For plates having the same mass/area, F is the relevant measure of strength at a given strain. For bilayers having the same mass/area, m_0 and subject to plane strain stretching,

$$\frac{F}{\sigma_R m_0 / \rho^m} = \left(1 + \frac{\rho^e h_0^e}{\rho^m h_0^m}\right)^{-1} \left[\frac{2}{3} S \sinh(2\varepsilon_1) + \frac{2}{\sqrt{3}} \left(\frac{2}{\sqrt{3}} \varepsilon_1\right)^N \right] e^{-\varepsilon_1} \quad (16)$$

A plot of the normalized force/length as a function of strain for a series of bilayers is presented in Fig. 5 for the same elastomer/steel combination considered above with $E/\sigma_R = 1/5$. The plot for the all-metal is

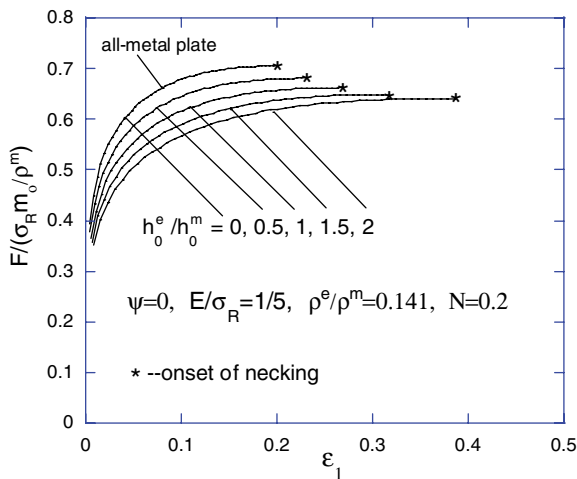


Fig. 5. Normalized force/length as a function of strain under plane strain tension for elastomer-metal bilayer plates having the same mass/area, including the all-metal plate. Necking starts at the maximum point indicated by the asterisk. Substituting elastomer for metal lowers the strength of the plate but increases the strain at which necking starts thereby, in this case, increasing the capacity of energy absorption.

included. The curves in Fig. 5 have been terminated at the onset of necking at the maximum load. After necking starts, F would fall sharply for relatively thin plates, and little additional energy would be absorbed beyond necking. Substitution of elastomer for steel reduces the strength of the bilayer plate. Nevertheless, the effect of this strength reduction on the plastic work is more than made up for by the increase in necking strain such that energy absorption in the bilayer exceeds that in the all-metal plate.

To illustrate the possible importance of neck retardation in the failure of bilayer plates, consider a bilayer with equal thickness layers ($h_0^e = h_0^m$) of an intermediate strength steel ($\sigma_R = 500$ MPa, $N = 0.2$) and an elastomer. For $S \approx 0.1$, the modulus of the elastomer must be $E \approx 50$ MPa. Experimental data on thermoplastic polyurethanes indicate that its modulus under quasi-static straining is $E = 66$ MPa (Amirkhizi et al., 2006; see also Qi and Boyce, 2005; Yi et al., 2006). Stress-strain data for polyurea (McGee et al., 2005; Yi et al., 2006) suggests a higher effective modulus at strain rates on the order of 10^3 /s, while data at even higher rates (Jiao et al., 2006) indicate much larger values of the modulus. Thus, it would appear that elastomers exist such that a bilayer should be capable of appreciably delaying the strain to failure (Figs. 1 and 2) and absorbing more energy in stretch (Fig. 4) than the corresponding all-steel plate of equal mass even under quasi-static stretching, at least for lower strength alloys.

In addition to ignoring material rate dependence, the analysis in this section is quasi-static. For high-rate stretching of rate-independent all-metal tensile specimens, Shenoy and Freund (1999) have shown that inertial effects retard necking and give rise to multiple necks. Numerical simulations of dynamic stretching of bilayer circular rings by L.B. Freund (unpublished work) and N. Wicks and J.W. Hutchinson (unpublished work) have given clear indications of the important role played by an elastomer layer in retarding necking under high strain rates: the higher the rate, the greater the delay in necking and the more necks in a given length of specimen. None of these simulations have accounted for material rate dependence. Hutchinson and Neale (1977) showed that strong material rate dependence results in neck retardation and the possibility of multiple necks under stretch rates sufficiently low that inertia can be neglected.

In an entirely different arena, the importance of quasi-static neck retardation in bilayers has also

recently been highlighted for very thin metal films bonded to thin polymer or elastomer substrates: metallization of flexible substrates in the electronics industry (Li and Suo, 2006). In this application the necking bands are at the micron scale. The result (10) when specialized to plane strain tension ($\psi = 0$) coincides with the result of Li and Suo, and the dimensionless combination S also emerged in their study.

3. Necking in circular bilayer plates subject to quasi-static pressure loading

In this section, neck development in plates under quasi-static lateral pressure loading is explored to obtain insights prior to studying impulsive lateral loadings. As in the previous section, it will be assumed that the materials comprising the bilayer remain bonded and are sufficiently ductile such that material damage does not occur prior to necking. The phenomenon will be studied by carrying out a numerical analysis of a specific problem (Fig. 6): a clamped, circular plate of radius R subject to uniformly distributed pressure p applied to the top surface of plate. Imperfections in the form of axisymmetric V-shaped grooves in the metal layer are introduced to create a slight reduction in local thickness. At the center location A, the imperfection is a shallow V-shaped depression. The circular plate, its

clamped support, the uniform pressure load, and the initial imperfection all have axial symmetry. The focus is on axisymmetric necks that develop from the initial imperfections. As shown in Fig. 6, the V-shaped imperfections are located at five locations marked A–E, at distances from the center that are 0, 1/5, 2/5, 3/5, 4/5 of the plate radius, R , respectively. The initial amplitude of the imperfection is denoted as a and its width is approximately $2h_0^m$. The elastomer layer is uniform. In all the computational results, $R = 0.5$ m and the initial thickness of the reference all-steel plate is taken to be $H_0^m = 0.01$ m. The criterion for necking is the condition that the thickness at the imperfection groove is reduced to one-half the current thickness at a representative point just outside of the necking zone. The representative point is chosen such that its distance to the groove tip is roughly two thickness of the metal layer.

The metal is taken to be representative of intermediate strength AH36 steel with a true tensile stress–strain curve

$$\begin{aligned} \sigma &= E^m \varepsilon, & \varepsilon &\leq \sigma_Y / E^m \\ \sigma &= \sigma_Y (E^m \varepsilon / \sigma_Y)^N, & \varepsilon &> \sigma_Y / E^m \end{aligned} \tag{17}$$

with $E^m = 210$ GPa, $\sigma_Y = 380$ MPa, $N = 0.17$ and Poisson ratio $\nu = 0.3$ (Lee and Wierzbicki, 2005). The reference stress defined in (1) as the stress at $\varepsilon = 1$ is $\sigma_R = 1.11$ GPa. The density of the steel is $\rho^m = 7800$ kg/m³.

The elastomer is representative of polyurea ($\rho^e = 1100$ kg/m³) and is modeled as a Mooney–Rivlin material allowing for slight compressibility (see Appendix). As in the previous section, comparisons will be made for bilayer plates having the same mass per initial area, $m_0 = 78$ kg/m², in (12). Two values of modulus will be used to study the effects, 66 MPa and 330 MPa. The choice $E = 66$ MPa is based on data for polyurea under quasi-static straining (Amirkhizi et al., 2006); $E = 330$ MPa will be used to illustrate an enhanced effect on modulus due to material strain rate in the dynamic calculations. Quasi-static results based on $E = 330$ MPa will also be presented for reference, even though this choice is almost certainly unrealistically large at low strain rates.

The computations are carried out using the finite strain version of ABAQUS Standard (2004). For all-metal plates and the metal layer of bilayer plates, four-node bilinear axisymmetric elements with reduced integration are used. Elements with width

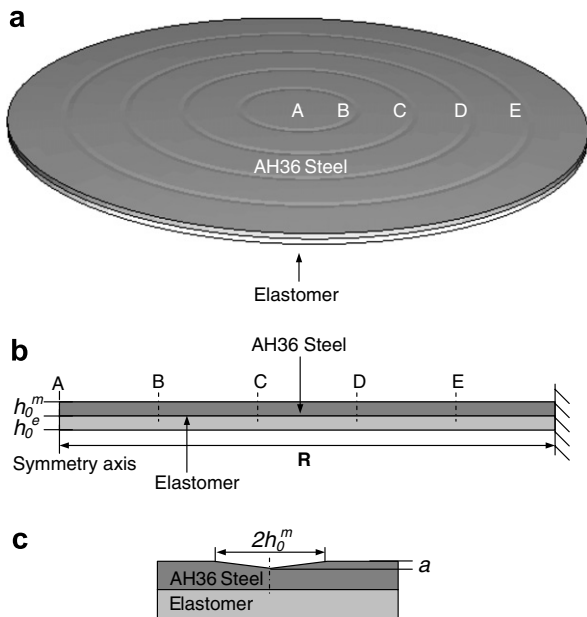


Fig. 6. Geometry of the circular plate, including locations of the initial axisymmetric imperfections at A–E.

of 0.5 mm are uniformly distributed through the whole plate, except at the locations of the imperfections where the elements are slightly distorted. For bilayer plates, three-node linear axisymmetric elements uniformly distributed through the whole layer are used to model the elastomer layer and each element has width of 0.5 mm. Selected calculations with further mesh refinement revealed that the mesh was adequate to accurately capture local necking behavior. The J_2 flow theory of plasticity, fit to the tensile stress–strain curve (17), was employed to represent the metal. The ABAQUS subroutine for Mooney–Rivlin materials was used to represent the elastomer (Appendix). Zero displacements are imposed at the plate edge. Several sets of calculations were performed to illustrate the influence of various factors on the plate performance, including the roles of the initial imperfection amplitude, the stiffness of the elastomer, and thickness ratio, h_0^e/h_0^m .

The role of imperfection amplitudes is first explored. The ratio of imperfection amplitude and metal layer thickness, a/h_m^0 , was varied to illustrate small (2.5%), medium (5%) and large (10%) imperfections. Fig. 7 presents deflection at the center of the plate as a function of the deflection at the center of the plate for an all-metal plate and a bilayer plate of the same mass/area. The bilayer plate has equal thickness of elastomer and metal layers and the modulus of the elastomer is 330 MPa. For both types of

plate, all five imperfections (at A–E in Fig. 6) are present with the same amplitude, and, in all cases shown in Fig. 7, necking occurs at location B. The results in Fig. 7 suggest that the overall strength of the bilayer plate is lower than the equivalent all-metal plate, consistent with the earlier results in Fig. 5, however, necking is retarded in the bilayer

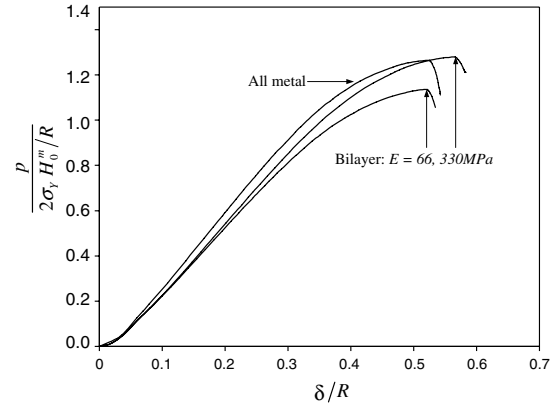


Fig. 8. Normalized pressure as a function of normalized deflection for all-metal steel plates and equal mass bilayer plates for two moduli of elastomer. A uniformly distributed pressure is applied to the top surface of each plate quasi-statically. The thicknesses of the metal and elastomer layers in the bilayer are equal. Initial imperfections for both cases have amplitudes: $a/H_0^e = a/h_0^m = 5\%$. Necking occurs at location B (see Fig. 10).

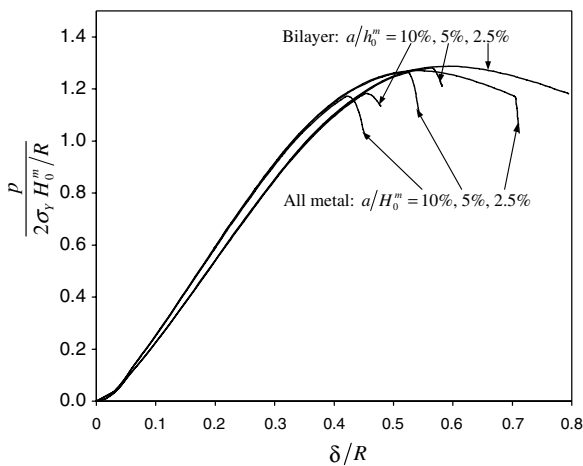


Fig. 7. Normalized pressure as a function of normalized deflection for all-metal steel plates and equal mass bilayer plates for three imperfection amplitudes. A uniformly distributed pressure is applied quasi-statically to the top surface of each plate. The thicknesses of the metal and elastomer layers in the bilayer are equal. The modulus of the elastomer is $E = 330$ MPa. Necking occurs at location B (see Fig. 10).

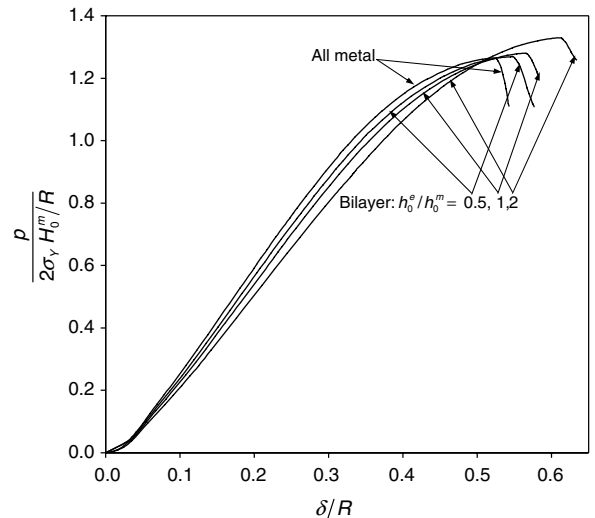


Fig. 9. Normalized pressure as a function of normalized deflection for all-metal steel plates and bilayer plates with three different thickness ratio of metal and elastomer layers. A uniformly distributed pressure is applied to the top surface of each plate quasi-statically. Initial imperfections for both cases have amplitudes: $a/H_0^e = a/h_0^m = 5\%$. The modulus of the elastomer is $E = 330$ MPa. Necking occurs at location B (see Fig. 10).

plates such that these plates are able to sustain larger deflections prior to the sudden drop in load.

The role of elastomer modulus ($E = 66$ MPa and $E = 330$ MPa) is demonstrated by Fig. 8, again for plates with the same mass/area, $m_0 = 78$ kg/m². Here, the imperfection amplitude is fixed at $a/h_0^m = 5\%$. The stiffer elastomer has a proportionally beneficial effect, increasing the plate overall strength and delaying neck growth for bilayer plates. There is no benefit for the bilayer with $E = 66$ MPa for imperfections this large, but the bilayer with $E = 330$ MPa is almost as strong as the all-metal plate and it necks at a deflection that is about 10% larger. As mentioned above, a modulus of $E = 330$ MPa ($E/\sigma_R = 0.3$) is unrealistically large for the quasi-static loading. Based on this example alone, one would conclude that there is

not any benefit under quasi-static loading for steel/polyurea bilayers if imperfections as large as 5% are representative.

Fig. 9 shows that the bilayer plate performance also depends on the thickness ratio of elastomer and metal layers, h_0^e/h_0^m , which are again constrained to have the same mass/area. The larger the relative thickness of elastomer layer, the smaller the overall strength of the plate, but the larger the neck retardation. All bilayer plates sustain larger pressure load at the onset of necking than the equivalent all-metal plate when the modulus is as large as $E = 330$ MPa, and the peak pressure increases with increasing the thickness ratio. The deformed configurations at necking for $h_0^e/h_0^m = 0, 0.5, 1$ and 2, are displayed in Fig. 10a–d, respectively. In all these cases, the neck develops at location B, in spite of fact

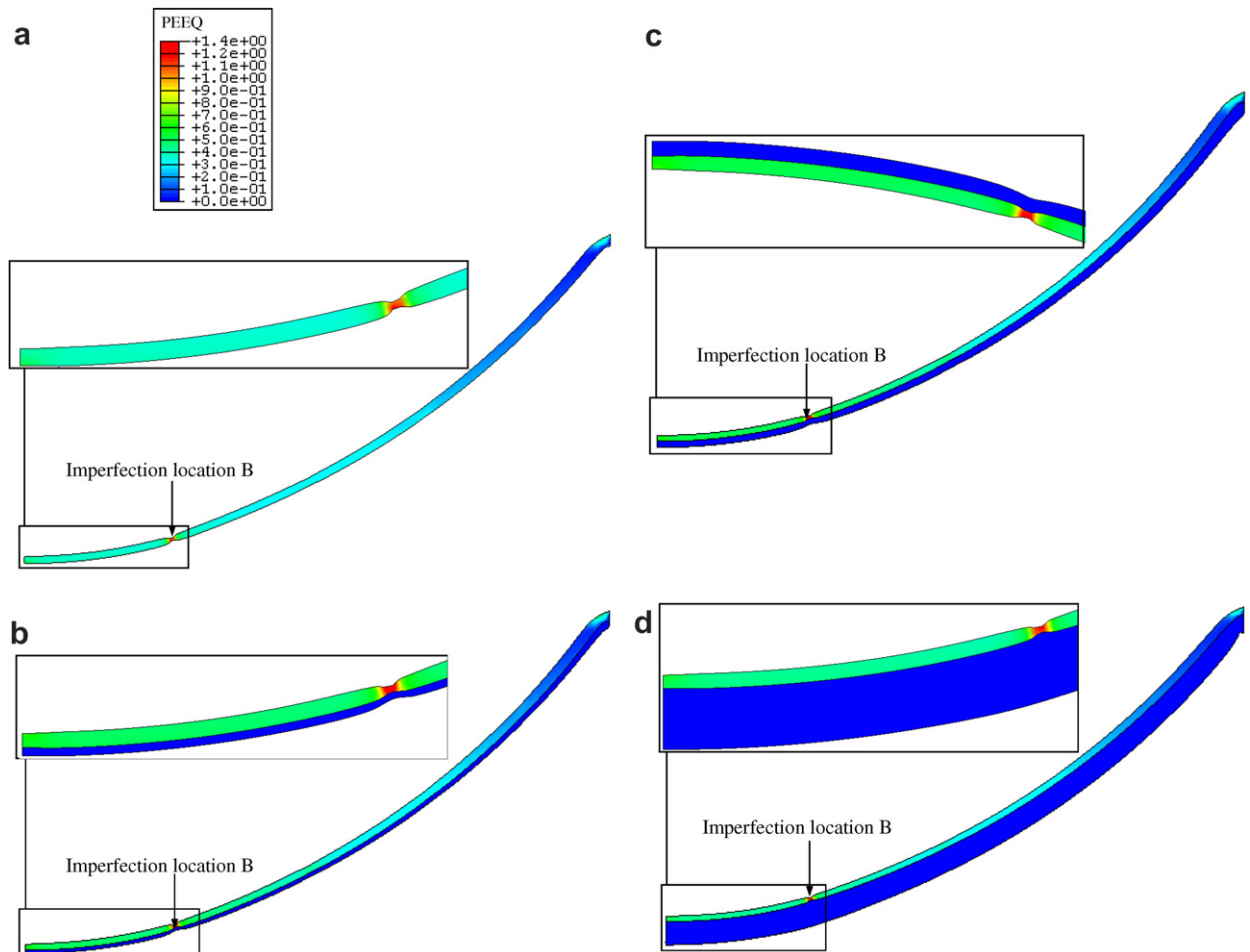


Fig. 10. Deformed configuration at the critical necking condition: (a) all-steel plates, (b) bilayer plate with $h_0^e/h_0^m = 0.5$, (c) bilayer plate with $h_0^e/h_0^m = 1$, (d) bilayer plate with $h_0^e/h_0^m = 2$, in each case with the same total mass per initial area. The modulus of the elastomer is $E = 330$ MPa. A uniformly distributed pressure is applied to the top surface of each plate quasi-statically. Initial imperfections for both cases have amplitudes: $a/H_0^m = a/h_0^m = 5\%$.

that the largest strain for the imperfection-free plate occurs at the center of the plate (location A). Calculations for a perfect plate reveal that the in-plane strain is largest at the center of the plate, diminishing gradually toward the edge. Fig. 1 reveals why the critical neck does not develop at the center of the plate. The state of strain at the center of the plate is equi-biaxial tension while that at the other imperfection locations is approximately in-plane plane strain tension. As seen in Fig. 1, the onset of necking under equi-biaxial tension occurs at significantly larger strains than under plane strain tension.

4. Necking in bilayer plates subject to dynamic loading

In this section, the question of whether neck retardation in bilayer plates persists under high intensity dynamic loadings is examined. The materials and geometry of the plates studied are the same as those described in the last section. The meshing schemes are also same as described earlier with mass distributed uniformly over the nodes. Two types of dynamic loadings are considered: an idealized uniform impulse and a time-dependent pressure loading focused at the center of the plate. A limited exploration of the directionality of the impulse will also be conducted. ABAQUS/Explicit (2004) is used to perform the computations.

4.1. Uniform impulsive loading

A uniformly distributed impulsive load is imparted as a uniform normal velocity, V , on all elements of the plate at $t = 0$, equivalent to an initial momentum/area, m_0V . A surviving plate must therefore absorb an initial kinetic energy/area, $\frac{1}{2}m_0V^2$. In the first set of results presented below, V is directed from the elastomer towards the steel, as if the blast were on the elastomer side of the plate (i.e. the elastomer is on the top in Fig. 6). The idealized loading is a reasonable approximation for meter-size plates subject to a uniform blast loading since the period of a representative pressure pulse is usually on the order of 10^{-4} s while the time for significant deflections to develop is on the order of several ms.

For a given all-metal plate with the five imperfections introduced in Fig. 6, a sequence of calculations is performed with increasing V until the critical value, V_{CR} , is reached such that the plate comes to rest (apart from elastic vibrations) with the neck-

ing criterion satisfied at one of the imperfection locations. As described earlier, the necking criterion requires the thickness at the critical groove be reduced to one-half of the current thickness at points just outside of the groove. Fig. 11 presents the deformed mesh configurations of plates at the critical velocity for the all-steel plate for three values of the imperfection amplitude, $a/H_0^m = 10\%$, 5% and 2.5%, which have the same amplitude at all five locations. The critical velocities are 170 m/s and 208 m/s for imperfection amplitudes of 10% and 5%, respectively, with the imperfection at location

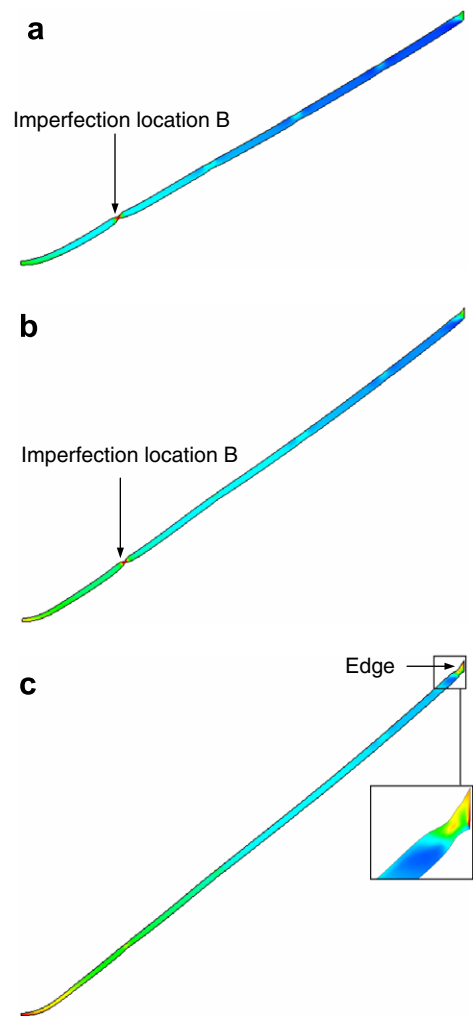


Fig. 11. Deformed configuration of all-steel plate at the critical necking condition under uniform initial impulsive loading: (a) $V_{CR} = 170$ m/s for an imperfection amplitude of $a/H_0^m = 10\%$; (b) $V_{CR} = 208$ m/s for an imperfection amplitude of $a/H_0^m = 5\%$; (c) $V_{CR} = 232$ m/s for an imperfection amplitude of $a/H_0^m = 2.5\%$.

B being the most deleterious. However, if the imperfection amplitude is as small as $a/H_0^m = 2.5\%$, necking first develops near the clamped edge at a critical velocity of 232 m/s. In this case, the constraint of the clamped support introduces local deformation which serves as an effective imperfection which is evidently more severe than the 2.5% imperfections at the other locations. Depending on the uniformity of the actual loading this may or may not be a realistic failure mode, as will be further clarified in the next subsection.

Deformed bilayer plates at necking subject to uniform impulsive loading are displayed in Fig. 12. These plates each have the same mass/area as the all-metal plate in Fig. 11, and they have equal elastomer and metal thicknesses with 5% imperfections at all locations. The critical velocity is 192 m/s for elastomer modulus $E = 66$ MPa, 201 m/s for $E = 198$ MPa, and 212 m/s for $E = 330$ MPa, respectively. In all these cases, the neck develops at location B, as was the case for the quasi-static loading. The elastomer bilayers under uniform impulse perform similarly to their all-metal counterpart with the same level of imperfection (e.g. $V_{CR} = 208$ m/s).

A different conclusion is reached for larger imperfections ($a/h_0^m = 0.1$) as seen in Fig. 13 showing deformed plates at necking and Fig. 14 with plots of the critical velocity required to cause necking as a function bilayer thickness ratio. As before, each location has the same imperfection amplitude, and the critical location is B in most cases, except that if the blast is directed towards to the elastomer side and $E = 330$ MPa, necking first develops near the clamped edge at a critical velocity of 178 m/s (Fig. 13d). A potential benefit is evident for bilayers with elastomer modulus, $E = 330$ MPa, but not with $E = 66$ MPa. The strain rate during much of the response of the plate is on the order of 10^3 s⁻¹, and thus a rate-enhanced modulus on the order of $E = 330$ MPa may not be unrealistic for simulation purposes under this loading. Included in Figs. 13 and 14 are two sets of results: one corresponding to the elastomer layer on the top (i.e. towards the blast) and the other with the elastomer layer on the bottom. There is a small, but not insignificant, dependence of the critical velocity on the placement of the elastomer, with elastomer towards the blast giving a slightly better performance. We have not been able to identify any mechanism leading to this difference, although perhaps that is not surprising given that the effect is small in these calculations. If the elastomer is towards the blast, its optimum

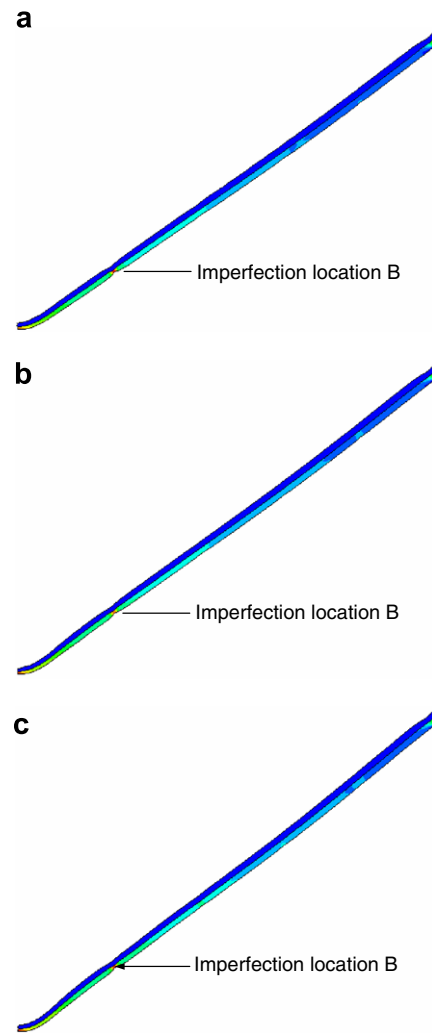


Fig. 12. Deformed configuration of bilayer plates with $h_0^e/h_0^m = 1$ at the critical necking condition for uniform impulsive loading: (a) $V_{CR} = 192$ m/s for $E = 66$ MPa; (b) $V_{CR} = 201$ m/s for $E = 198$ MPa; (c) $V_{CR} = 212$ m/s for $E = 330$ MPa. The blast is directed towards to the elastomer side. Initial imperfections at all locations have $a/H_0^m = a/h_0^m = 5\%$.

bilayer has roughly equal thicknesses of elastomer and steel.

4.2. Non-uniform impulsive pressure loading

The fact that the relative benefit of the bilayer appears to hinge on the amplitude of the imperfection for uniform impulses raises the question whether non-uniform loading might manifest itself in a fashion similar to a large imperfection. To answer this question, we considered the case where an intense non-uniform pressure focused on the

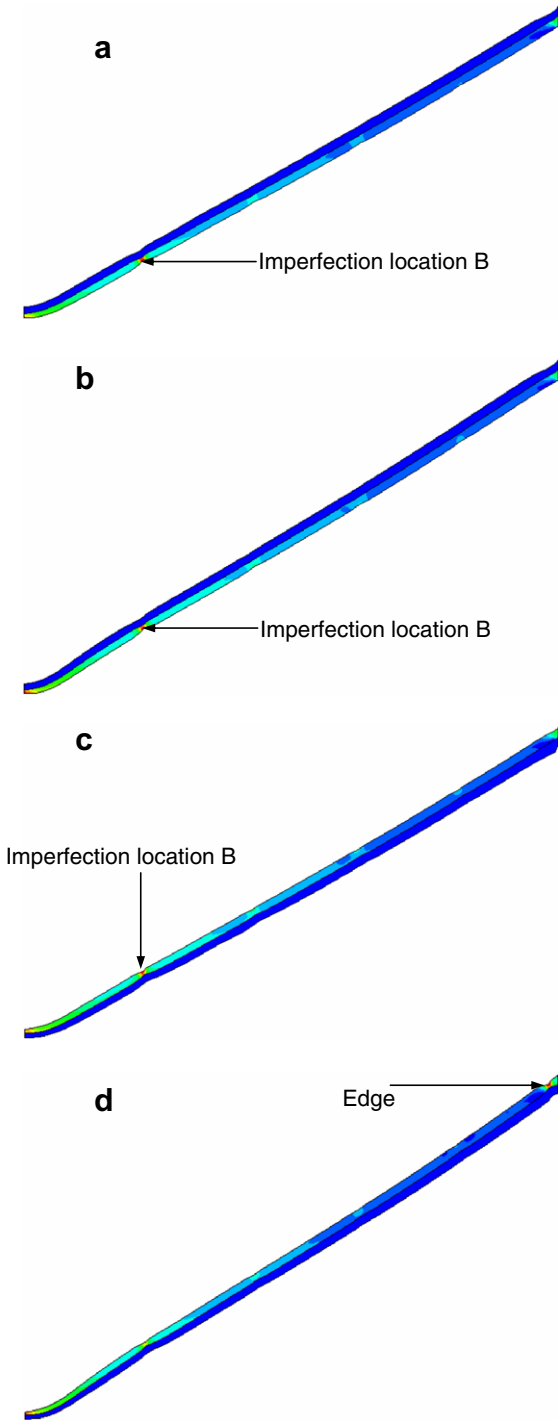


Fig. 13. Deformed configuration of bilayer plates with $h_0^c/h_0^m = 1$ at the necking condition for uniform impulsive loading: (a) $V_{CR} = 155$ m/s and $E = 66$ MPa; (b) $V_{CR} = 169$ m/s and $E = 330$ MPa; (c) $V_{CR} = 158$ m/s and $E = 66$ MPa; (d) $V_{CR} = 178$ m/s and $E = 330$ MPa. The elastomer is on the top side for cases (a) and (b) while it is on the bottom side for (c) and (d). All locations have imperfection amplitude, $a/H_0^m = 10\%$.

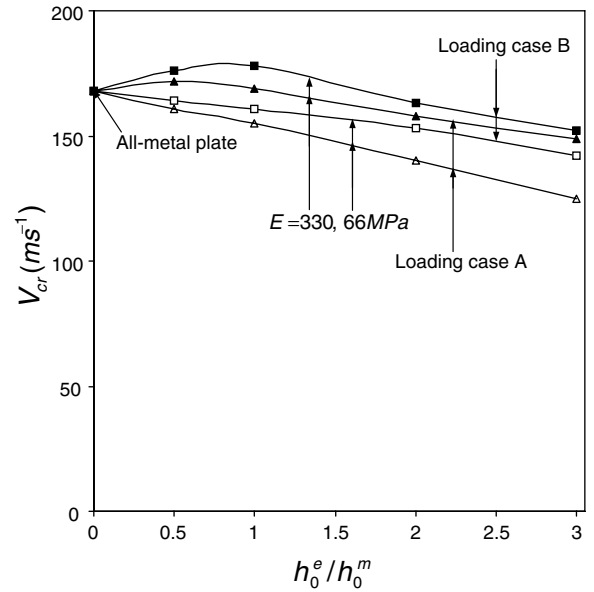


Fig. 14. Critical velocity for all-metal steel plates and equal mass bilayer plates for two values of the elastomer Young’s modulus. The loading is an initial, uniformly distributed momentum/area, $m_0 V_{CR}$. Loading case A has elastomer on top and case B has elastomer on bottom. In each case the impulse is directed downward.

central region of the plate is applied for a period of time that is short compared to the response period of the plate. The axisymmetric pressure distribution profile is given by

$$p(r, t) = P e^{-(r/d)^2} e^{-t/t_d} \tag{18}$$

where P is the peak pressure, r is measured from the center of the plate, and $d = 0.2$ m and $t_d = 10^{-4}$ s are used in the calculations. The choice $d = 0.2$ m produces a pressure acting on the central region of the plate, extending out to about 1/3 of the distance to the edge. Separate calculations are carried out for the pressure applied to each side of the bilayer.

The critical pressure P_{CR} is defined to be the minimum peak pressure required to attain the necking condition stated earlier at any of the five imperfection locations. To identify the critical pressure for each case, a sequence of calculations is carried out, starting with P below P_{CR} , until a value of P is reached where the plate meets the necking criterion, analogous to the procedure used in previous section for identifying the critical velocity. The initial imperfection amplitude at all five locations in Fig. 1 is taken to be the smallest of the values used previously, $a/h_0^m = 2.5\%$.

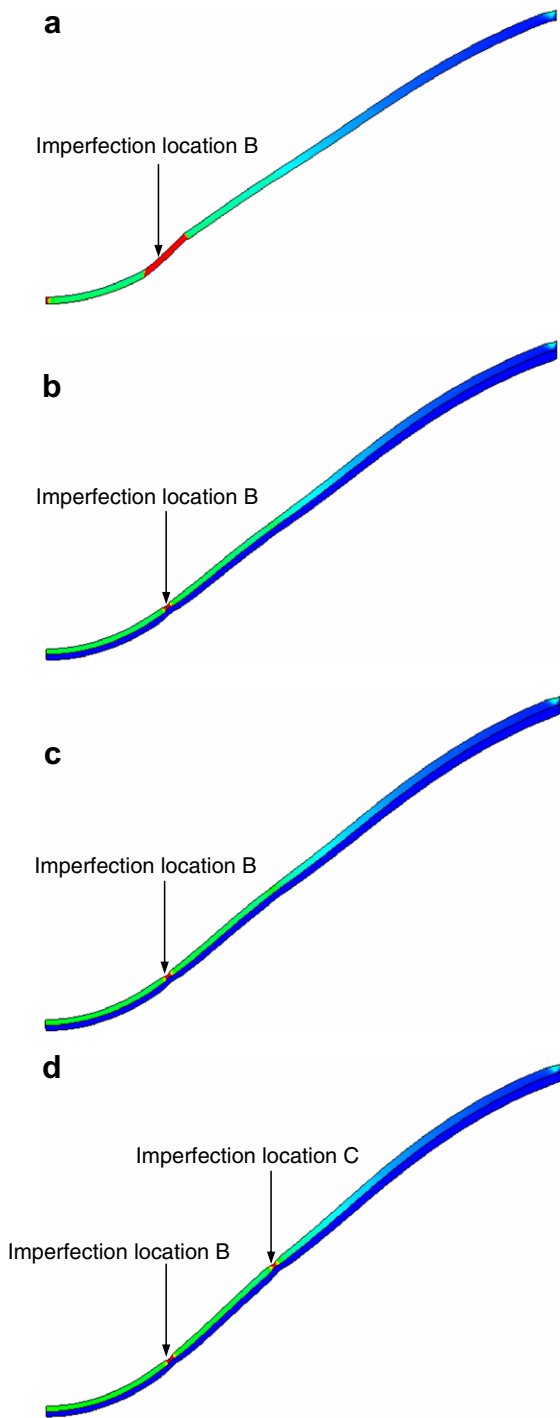


Fig. 15. Deformed configuration at the necking for pressure impulse localized at the center of the plate: (a) all-steel plate, $P_{CR} = 490$ MPa; (b) bilayer plate with $E = 66$ MPa, $P_{CR} = 510$ MPa; (c) bilayer plate with $E = 198$ MPa, $P_{CR} = 540$ MPa; (d) bilayer plate with $E = 330$ MPa, $P_{CR} = 580$ MPa. All plates have the same mass/area and imperfections with amplitudes $a/H_0^m = a/h_0^m = 2.5\%$. The bilayers have $h_0^e/h_0^m = 1$ with pressure is applied to the steel side.

Fig. 15 shows the deformed configuration at the critical pressure for an all-steel plate and bilayer plates having equal thickness ratio of elastomer and steel layers and three different elastomer moduli. The critical pressure for all-steel plate is $P_{CR} = 490$ MPa, while for bilayer plates: $P_{CR} = 510$ MPa for $E = 66$ MPa, $P_{CR} = 540$ MPa for $E = 198$ MPa and $P_{CR} = 580$ MPa for $E = 330$ MPa, respectively. The critical location in each instance is location B, but for the bilayer with the largest elastomer modulus ($E = 330$ MPa) a second neck has developed simultaneously at C. The calculations shown in Fig. 14 were repeated with the pressure acting on the elastomer side of the bilayer. The critical pressures obtained were almost identical to those quoted above for the case where the pressure acts on the steel side of the bilayer. Finally, it can be noted that the neck in the all-metal plate is highly stable, spreading over multiple thicknesses of the plate. This is believed to be a consequence of inertial stabilization (Shenoy and Freund, 1999) which will be explored in subsequent work, along with other aspects of dynamic neck development.

A substantial benefit of bilayer plates over all-metal plates of the same mass emerges under the non-uniform loading, even for small imperfection levels and relatively low values of the elastomer modulus. Under the uniformly distributed impulse, the bilayers were seen to be beneficial only when the imperfections are relatively large. It appears that the non-uniform loading acts in much the same way as a large imperfection in inducing necking.

5. Conclusions and issues for further study

The role of the elastomer in retarding necking that emerges from this study is fairly complicated. Under quasi-static loading, bilayers comprised of an elastomer layer bonded to a ductile metal layer can undergo appreciably greater stretch prior to necking than an all-metal plate if the stiffness/strength parameter satisfies $S = h_0^e E / (h_0^m \sigma_R) \geq 0.1$. Moreover, an elastomer/steel bilayer (with $\rho^e / \rho^m \cong 0.14$) will absorb more energy prior to necking than an all-steel plate of the same mass/area if $E / \sigma_R > 0.1$. It is essential that the incremental modulus of the elastomer in the above criteria be that associated with strains in the necking range of the bilayer. Any erosion of this modulus in this range would reduce the effect. These two simple criteria represent lowest order requirements for enhanced performance

of a bilayer relative to the corresponding all-metal plate. They are based on a quasi-static bifurcation analysis for the onset of necking, analogous to the Considere necking criterion in uniaxial tension. They do not take into account initial imperfections in either the geometry of the plate or in the material properties, nor do they account for inertial or material rate effects.

The axisymmetric analysis of a clamped circular plate subject to a *uniform impulsive load* suggests that there is not much benefit to be gained from a elastomer/steel bilayer compared to an all-metal plate unless the plate has fairly large thickness imperfections and the effective modulus of the elastomer satisfies $E/\sigma_R > 0.3$. On the other hand, the same plates subject to a *non-uniform impulsive load* focused at the center of the plate show a distinct advantage of the bilayer over the all-metal plate even when the imperfections are small and the elastomer modulus is as low as $E/\sigma_R \sim 0.1$. The non-uniformity of the loading appears to have an effect on necking analogous to a large imperfection. For the non-uniform loading, the critical impulse required to meet the necking condition was not found to depend on the location of the elastomer relative to the blast. For the uniform impulses, a slight dependence on the placement of the elastomer layer was noted.

These findings are subject to the following caveats. Material rate effects have not been taken into account, neither for the metal or, more importantly, for the elastomer. As an approximation, the modulus of the elastomer and the reference stress of the metal in Section 4 should be identified with strain rates relevant to the rate of deformation and strains relevant to necking. For meter-scale plates, the strain rate typically lies in the range from 100 s^{-1} to 1000 s^{-1} ; the effective stiffness of an elastomer can be substantially greater at these rates than under quasi-static stretching (Amirkhizi et al., 2006; Jiao et al., 2006; McGee et al., 2005; Yi et al., 2006). However, a crude approximation of this type may miss another important contribution of material rate dependence to neck retardation. By its nature, necking gives rise to larger strain rates within a developing neck than outside it. Consequently, positive material rate dependence, which elevates stress due to increased strain rate, will tend to slow down the growth of the neck (Hutchinson and Neale, 1977). Further experimental work is needed to establish realistic rate dependent material models, and studies with such models should show

whether the retardation and energy absorption effects displayed in this paper are realistic.

The mechanism of neck retardation requires the elastomer to remain bonded to the metal. Debonding in the vicinity of the developing neck will cause load to be shed to the neck in the metal layer and retardation will be lost. The interaction between debonding and necking has been investigated by Li et al. (2005) for the complementary problem of a thin metal film on an elastomer substrate under quasi-static straining.

The quasi-static results for the onset of necking are based on a bifurcation analysis for a bilayer with no imperfections. The study of axisymmetric neck development in the dynamically loaded circular plate included imperfections in the form of initially thinned regions at several locations. The most susceptible locations were those near the center of the plate where the strains are the largest. Particularly for the uniform impulsive loading, the conclusions related to the potential benefit of the bilayer depended strongly on the amplitude of the imperfection. Imperfections play a critical role in dynamic stability problems such as necking, influencing both the location of the necks as well as their rate of growth (Shenoy and Freund, 1999). Further work along these lines is also needed to understand the performance of the bilayers.

Finally, the working assumption in the present study has been that the metal is sufficiently ductile that pronounced necking occurs prior to material damage in the form of void nucleation and growth or micro-cracking. For some metal alloys, this is a reasonable assumption, however, for others, damage is expected to develop along with the growth of the neck and contribute to the localization process. Furthermore, the employment of an elastomer layer to retard necking makes it more likely that damage and necking will occur simultaneously. Thus, studies which account for damage in the constitutive response of the metal should further elucidate the phenomenon considered here. Even if material damage contributes to localization, an elastomer layer may still be useful in retarding the localization.

Acknowledgements

The authors acknowledge contributions of L.B. Freund to this study; he was the first to explore the role of the elastomer in the bilayer in retarding necking, and his unpublished work on the dynamic

expansion of metal–elastomer rings revealed enhanced overall stretching. We are also indebted to R.J. Clifton and T. Jiao who raised a number of questions concerning the circular plate study in the first version, which has been completely revised. This work was supported in part by ONR Grant N00014-04-1-0154 and in part by the Division of Engineering and Applied Sciences, Harvard University.

Appendix

A modification of the Mooney–Rivlin material to allow slight compressibility is available in **ABAQUS Explicit (2004)**. It is summarized here, and experimental values for the coefficients for polyurea are reported from **Amirkhizi et al. (2006)**. The strain energy potential is

$$W = C_{10}(\bar{I}_1 - 3) + C_{01}(\bar{I}_2 - 3) + D(J - 1)^2 \quad (19)$$

where W is the strain energy per initial volume; C_{10} , C_{01} , and D are material parameters. Strain invariants are defined as

$$\begin{aligned} \bar{I}_1 &= \bar{\lambda}_1^2 + \bar{\lambda}_2^2 + \bar{\lambda}_3^2 \quad \text{and} \\ \bar{I}_2 &= \bar{\lambda}_1^{(-2)} + \bar{\lambda}_2^{(-2)} + \bar{\lambda}_3^{(-2)} \end{aligned} \quad (20)$$

where λ_i are the principal stretches, $\bar{\lambda}_i = J^{-1/3}\lambda_i$ are the modified stretches, and J is the ratio of the deformed volume to the undeformed volume. Thermal effects are not taken into account. The initial shear modulus, Poisson's ratio, Young's modulus and bulk modulus are given by

$$\begin{aligned} \mu &= 2(C_{10} + C_{01}), \quad E = 2(1 + \nu)\mu \quad \text{and} \\ K &= 2D \end{aligned} \quad (21)$$

In the numerical study in Sections 3 and 4, coefficients are chosen based in part on values provided by **Amirkhizi et al. (2006)** for polyurea. To explore the effect of the initial Young's modulus (or, equivalently, the initial shear modulus), three sets of coefficients have been used: $C_{10} = 10.7$ MPa, $C_{01} = 0.423$ MPa, $D = 393$ MPa, correspond to initial shear modulus of $\mu_0 = 22.2$ MPa, initial Young's modulus of $E = 66$ MPa and Poisson's ratio of $\nu = 0.486$; $C_{10} = 32.1$ MPa, $C_{01} = 1.27$ MPa, $D = 1180$ MPa,

correspond to initial shear modulus of $\mu_0 = 66.7$ MPa, initial Young's modulus of $E = 198$ MPa, and Poisson's ratio of $\nu = 0.486$; $C_{10} = 53.5$ MPa, $C_{01} = 2.11$ MPa, $D = 1967$ MPa, correspond to initial shear modulus of $\mu_0 = 111$ MPa, initial Young's modulus of $E = 330$ MPa, and Poisson's ratio of $\nu = 0.486$. The density of the polymer is $\rho_p = 1100$ kg/m³.

References

- ABAQUS/Explicit User's Manual Version 6.5, 2004. ABAQUS Inc.
- ABAQUS/Standard User's Manual Version 6.5, 2004. ABAQUS Inc.
- Amirkhizi, A.V., Isaacs, J., McGee, J., Nemat-Nasser, S., 2006. An experimentally-based viscoelastic constitutive model for polyurea, including pressure and temperature effects. *Philos. Mag.* 86, 5847–5866.
- Hutchinson, J.W., Neale, K.W., 1977. Influence of strain-rate sensitivity on necking under uniaxial tension. *Acta Met.* 25, 839–846.
- Hutchinson, J.W., Neale, K.W., 1978. Sheet Necking – II. Time-independent behavior. In: Koistinen, D.P., Wang, N.-M. (Eds.), *Mechanics of Sheet Metal Forming*. Plenum Publishing Corporation, pp. 127–153.
- Jiao, T., Clifton, R.J., Grunschel, S.E., 2006. High Strain rate response of an elastomer. In: *The Proceedings of the Conference of the American Physical Society Topical Group on Shock Compression of Condensed Matter*, 2005, American Institute of Physics, vol. 845, pp. 809–812.
- Lee, Y.W., Wierzbicki, T., 2005. Failure prediction of thin plates under localized impulse loading. Part II: Discing and petaling. *Int. J. Impact Eng.* 31, 1277–1308.
- Li, T., Suo, Z., 2006. Deformability of thin metal films on elastomer substrates. *Int. J. Solid Struct.* 43, 2351–2363.
- Li, T., Huang, Z.Y., Lacour, S.P., Wagner, S., Suo, Z., 2005. Delocalization strain in a thin metal film on a polymer substrate. *Mech. Mater.* 37, 261–273.
- McGee, J., Issacs, J., Nemat-Nasser, S., 2005. An interim report on experimental results for modeling high strain-rate properties of polyurea at large compressive strains. USCD-Center of Excellence for Advanced Materials.
- Qi, H.J., Boyce, M.C., 2005. Stress–strain behavior of thermo-plastic polyurethanes. *Mech. Mater.* 37, 817–839.
- Shenoy, V.B., Freund, L.B., 1999. Necking bifurcations during high strain rate extension. *J. Mech. Phys. Solids* 47, 2209–2233.
- Storen, S., Rice, J.R., 1975. Localized necking in thin sheets. *J. Mech. Phys. Solids* 23, 421–441.
- Yi, J., Boyce, M.C., Lee, G.F., Balizer, E., 2006. Large deformation rate-dependent stress–strain behavior of polyurea and polyurethanes. *Polymer* 47, 319–329.